Emission Spectra and Self-Terminating Lasers of Electron-Beam-Produced Rare Gas Plasmas

By

Kouichi ONO,* Goro KAMIMOTO** and Kuniya FUKUDA***

(Received December 27, 1979)

Abstracts

Plasmas of rare gases (He through Xe) were produced by a short-pulsed, high-current electron beam (600 kV, 10 kA peak, 3 ns FWHM) in a drift tube without an external field over a wide range of pressure (0.1～80 Torr). Emission spectra of the plasmas were observed between 2500 and 8500 Å with a spectrograph and band-pass filters in the directions of end- and side-on views. Short-pulsed laser emissions (3 ns FWHM, 10～400 W peak) traveling along with the electron-beam pulse were found for 20 spectral lines of singly-ionized and neutral Ne, Ar, Kr, and Xe atoms through the end window of the drift tube. The small signal gain coefficients were measured. Temporal behaviors of the emission intensity were observed for the laser lines as well as for many other spontaneous lines through the side window. The atomic processes for the laser excitations have been examined.

§ 1. Introduction

Many authors have investigated plasmas produced by the injection of a pulsed high-current electron beam (an intense relativistic electron beam: REB) into neutral gases or discharge-preformed plasmas in a drift tube. (See refs. of a previous paper[1]). However, only a few works have been performed to reveal the spectroscopic natures of the plasmas. Rizzo[2] observed a successive ionization of Ar atoms to ArII through IV in the Ar plasma. Wei *et al.*[3] observed the difference between the air plasmas under self-focused and unfocused electron-beam conditions, i. e., spectra of OII, NII, and NIII under the former, and those of N_2-2nd-positive under the latter. Other investigators measured some emission lines to monitor the plasma conditions, *e. g.*, the H_α and H_β lines in the H plasma,[4-6] and the HeI 4921 and HeII 4685 Å lines in the He plasma.[7-10]

* Department of Aeronautical Engineering.
** Department of Mechanical Engineering, Aichi Institute of Technology, Toyota, Aichi.
*** Department of Engineering Science.

As for laser oscillations by electron-beam excitation, extensive works have been carried out on excimer lasers[11,12] at high pressures, and on molecular lasers of H_2, HD, and D_2,[13-16] CO,[13] and N_2[13,16-19] at low pressures. However, only the works by Dreyfus *et al.*[13,16] were concerned with lasers of ionized and neutral atomic lines in the Ne plasma excited at low pressures.

The present investigations have been conducted as one of our studies which aim to reveal the production mechanism and nature of plasmas produced by the injection of a short-pulsed, high-current electron beam (600 kV, 10 kA peak, 3 ns FWHM) into various neutral gases in a drift tube without an external magnetic field. In the previous paper,[1] one of the present authors measured the radial configurations of the axial plasma current induced by the electron beam in H_2, N_2, and rare gases (He through Xe). He showed that the plasma current persisted in the initial total-current (beam and plasma currents) configuration for a rather long time up to 2 μs after the passage of the beam pulse, depending on the gas pressure. Furthermore, he found the emissions of the high-iniensity visible and ultraviolet spectral lines of NeI, NeII, ArII, KrII, and XeII traveling along with the electron-beam propagation.[20]

The present paper is concerned with the observations of light emissions from the electron-beam-produced rare gas (He through Xe) plasmas in the spectral region between 2500 and 8500 Å. Photographic as well as photoelectric observation were carried out in both directions of end- and side-on views of the plasmas over a wide range of gas pressure. This paper especially describes in detail the behaviors of the self-terminating laser oscillations of the spectral lines belonging to singly-ionized and neutral Ne through Xe atoms. In the next section, the experimental procedures are described, and in § 3, the experimental results are presented on the end- and side-on observations. The small signal gain coefficients are determined for the laser emissions traveling along with the electron-beam pulse. In the last section, the experimental results of the singly-ionized laser lines are compared with those of many other spontaneous lines. Lastly, the atomic processes for the laser excitations are discussed in connection with the behaviors of the plasma current.

§ 2. Experimental Procedure

As the experimental procedures were almost the same as those reported in the previous paper[1], only pertinent descriptions are given here. An electron beam (600 kV, 10 kA peak, 3 ns FWHM, and 3 cm dia.) produced by a Febetron 706 (Field Emission Corp.) was injected into neutral gas of He (2.5~80 Torr), Ne (0.8~30 Torr), Ar (0.3~8 Torr), Kr (0.2~4 Torr), or Xe (0.1~3 Torr) through a 50 μm thick Mylar entrance window of a drift tube (120 cm total length and 12.6 cm inner dia.). The drift tube consisted of a Pyrex tube (100 cm length), stainless-steel

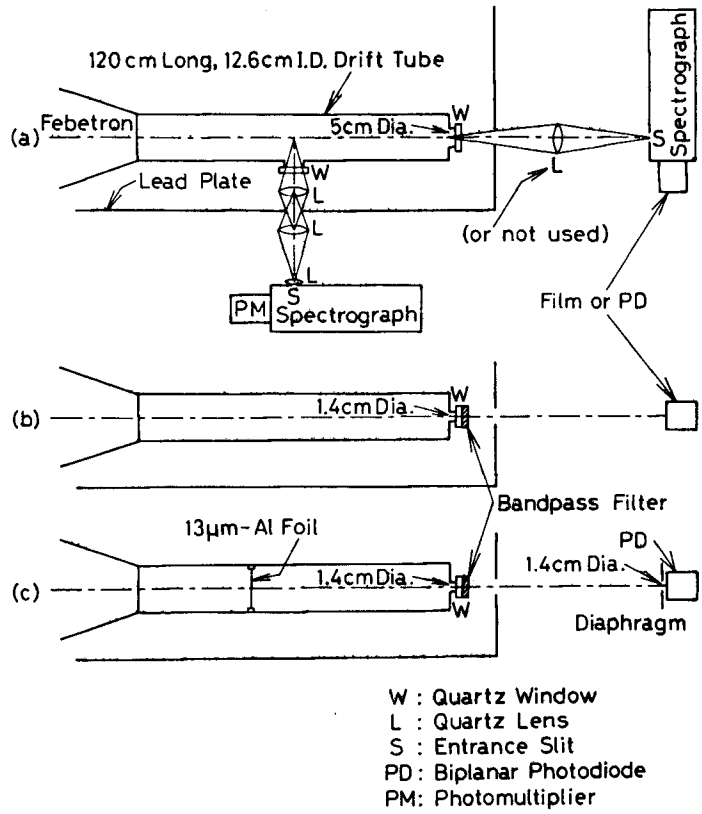

Fig. 1. Experimental setups for (a)—(c) end-on and (a) side-on observations.

adapters, and a copper mesh around the Pyrex tube.

Figure 1(a) shows the experimental setup for a spectroscopic observation of light emissions from the plasma in the spectral region between 2500 and 8500 Å with a spectrograph of 100 cm Ebert mounting (Shimadzu GE-100) having a grating of 2160 lines/mm (3000 Å blaze) or 1200 lines/mm (5000 Å blaze). The end-on view spectra were observed with high-speed photographic films(Kodak 2475-Recording and 2481-High-Speed-IR) or with a biplanar photodiode (HTV R617U) through a quartz window of 5 cm diameter at the end of the drift tube. There, a point on the tube axis inside the end window was focused by a condensing lens on the entrance slit of the spectrograph. The side-on view spectra were observed with photomultipliers (Philips 56AVP, and HTV 1P28 and R666) through a quartz window of 1.4 cm diameter attached to the drift-tube wall at 58 cm from the entrance window. There, a point on the tube axis was focused on the entrance slit of the spectrograph by three condensing lenses.

Figures 1(b) and (c) show the experimental setups for an end-on observation of

light emissions with bandpass interference filters (50～120 Å $\Delta\lambda_{1/2}$) through a quartz window of 1.4 cm diameter attached to the end of the drift tube. (b) The time-integrated emission pattern was photographed with high-speed films, and the intensity was measured with a biplanar photodide. (c) A 13 μm thick aluminum foil, supported between two Lucite circular plates of 12.4 cm diameter with an aperture of 10.4 cm diameter, was set in the drift tube, and the intensity of the emission from the plasma between the foil and the end window was measured with a biplanar photodiode. Here, a diaphragm with an aperture of 1.4 cm diameter was set in front of the photodiode.

Wavelengths of spectral lines photographed with the spectrograph were determined within an accuracy of 0.5 Å and identified with refs. 21-23. The relative sensitivities in the wavelength of the spectrograph with the photographic films and with the photomultipliers were calibrated with a standard tungsten-ribbon lamp. However, the relative sensitivity with the photodiode was not calibrated due to its poor sensitivity. The absolute sensitivity of the photodiode was assumed to be a typical spectral response curve for the combination of a multi-alkali photosurface and a UV-grade-glass entrance window of the photodide. The transmissivities of the bandpass filters were calibrated with the spectrograph and tungsten-ribbon lamp. All time-resolved signals were observed on oscilloscopes. The time responses of the detection systems with the photodiode and with the photomultipliers were about 2 and 3 ns, respectively.

In order to monitor the experimental reproducibility from shot to shot of the Febetron, a side-on view picture of light emission for each shot was photographed with an open-shutter camera.[1] The azimuthal magnetic field was measured with a magnetic

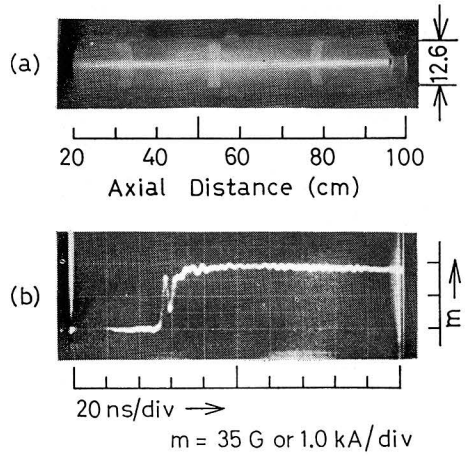

Fig. 2. (a) Open-shutter photograph of side-on light emission in the 3000～7000 Å spectral region and (b), oscilloscope trace of the azimuthal magnetic field on the drift-tube wall at 1.5 Torr for Ar.

loop coil on the drift-tube wall at 58 cm from the entrance window.[1] Figures 2(a) and (b) show some typical examples of these observations for the monitoring.

§ 3. Experimental Results

3. 1 End-on observation

Figure 3(a) shows some typical examples of space-resolved and time-integrated spectra of light emissions from the plasmas at 1.5 Torr for Ar and at 0.5 Torr for Xe in the spectral region between 4100 and 4700 Å. The full lengths d of the spectrograms correspond to the diameter of 5 cm centered at the drift-tube axis. The bright inner spectra correspond to the bright region of the light emission along the tube axis in Fig. 2(a). The inner spectra consist of singly-ionized and neutral atomic lines on a weak continuum, among which there are high-intensity ArII 4277 and XeII 4296 Å lines. The gloomy outer spectra consist mainly of neutral lines. When the condensing lens was taken away and the entrance slit of the spectrograph was set sufficiently far from the end window (100 cm or so), only the high-intensity lines were photographed, as shown in Fig. 3(b). The spectra (a) and (b) were both photographed in one Febetron shot with the spectrograph at 120 cm from the

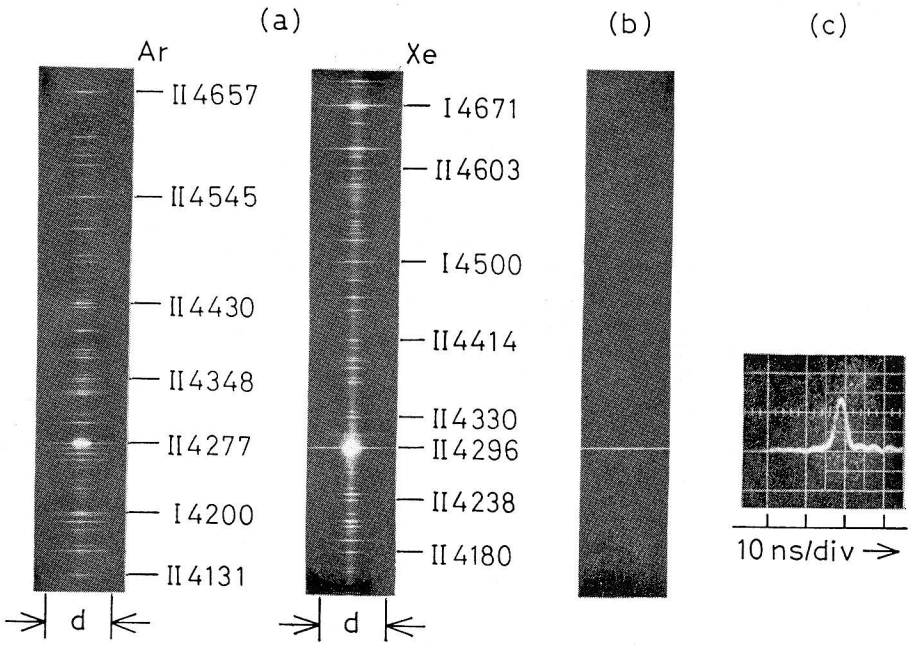

Fig. 3. End-on observations at 1.5 Torr for Ar and at 0.5 Torr for Xe. Time-integrated spectra photographed at 120 cm from the end window (a) with, and (b) without, the condensing lens. (c) Oscilloscope trace of the emission of the high-intensity line.

end window (Fig. 1(a)). The spectra for Ne and Kr, which also included some high-intensity lines, showed almost the same appearances as those for Ar and Xe, except for the disappearance of the weak continuum in the Ne spectra. The He spectra consisted of HeI lines and a very weak HeII 4685 Å line.

In the photoelectric observation with the spectrograph and photodiode (Fig. 1(a)), only the high-intensity spectral lines were detected, and showed a pulse with a FWHM of 3 ns or less as shown in Fig. 3(c). This pulse appeared at the end of the drift tube almost simultaneously with the electron-beam pulse, i. e., the 4870 Å light pulse (about 2 ns FWHM) emitted from a ZnSe target bombarded by the electron beam at the end window.

The observed high-intensity spectral lines are listed in Table I for Ne, Ar, Kr, and Xe. For He there were no such intense lines. As indicated in the Refs. in this table, most of these lines have been reported as self-terminating laser lines, which were observed in plasmas produced by electron-beam propagation,[13,16] traveling-wave

Table I. High-intensity spectral lines observed in the direction of end-on view.

Identification (Lower-Upper)		λ (Å)	Maximum Intensity			Refs.
			P_{IM} (Torr)	I_{IM} (W)	α (cm^{-1})	
Singly-Ionzed Atomic Lines						
NeII	$3s'^2D_{3/2}-3p'^2P^o_{1/2}$	3319.7	10	10	0.048	13, 16
NeII	$3s^2P_{3/2}-3p^2P^o_{3/2}$	3323.7	10	69		13, 16, 26, 35
NeII	$3s'^2D_{5/2}-3p'^2P^o_{3/2}$	3345.4	10	64		
NeII	$3s^2P_{1/2}-3p^2P^o_{1/2}$	3378.2	10	25		
ArII	$4p^4P^o_{1/2}-4d^4D_{1/2}$	3509.7	3	29	0.067	
ArII	$4s'^2D_{5/2}-4p'^2P^o_{3/2}$	4277.5	2.5	47	0.069	
KrII	$5p^4P^o_{3/2}-5d^4P_{1/2}$	3771.3	1.5	240	Sat.	26
KrII	$5s'^2D_{3/2}-5p'^2P^o_{1/2}$	4057.0	—	~3	—	
KrII	$5s'^2D_{5/2}-5p'^2P^o_{3/2}$	4475.0	—	~3	—	
KrII	$5s^4P_{5/2}-5p^4P^o_{3/2}$	4658.8	1.5	57	Sat.	
XeII	$6p^4P^o_{3/2}-7s^4P_{1/2}$	4296.4	1	84	Sat.	26
XeII	$5d^2D_{5/2}-6p'^2P^o_{3/2}$	4972.7	—	~2	—	26
Neutral Atomic Lines						
NeI	$3s[3/2]^o_1-3p'[1/2]_0$	5400.5	20	80	0.040	*
NeI	$3s[3/2]^o_2-3p[3/2]_2$	6143.0	6	79	0.031	**
ArI	$4s[3/2]^o_2-4p[3/2]_1$	7723.7	2	71	0.017	
ArI	$4s'[1/2]^o_0-4p'[1/2]_1$	7724.2				
ArI	$4s'[1/2]^o_0-4p'[3/2]_1$	7948.1	2	46	0.052	
KrI	$5s[3/2]^o_2-5p[3/2]_2$	7601.5	1	29	0.038	34
KrI	$5s[3/2]^o_2-5p[5/2]_2$	8104.3	1.5	440	Sat.	26, 28
XeI	$6s[3/2]^o_2-6p[3/2]_1$	8409.1	0.8	23	0.015	28

* 24, 25, 27, 29–32, 35. ** 25, 26, 30–33, 35, 36.

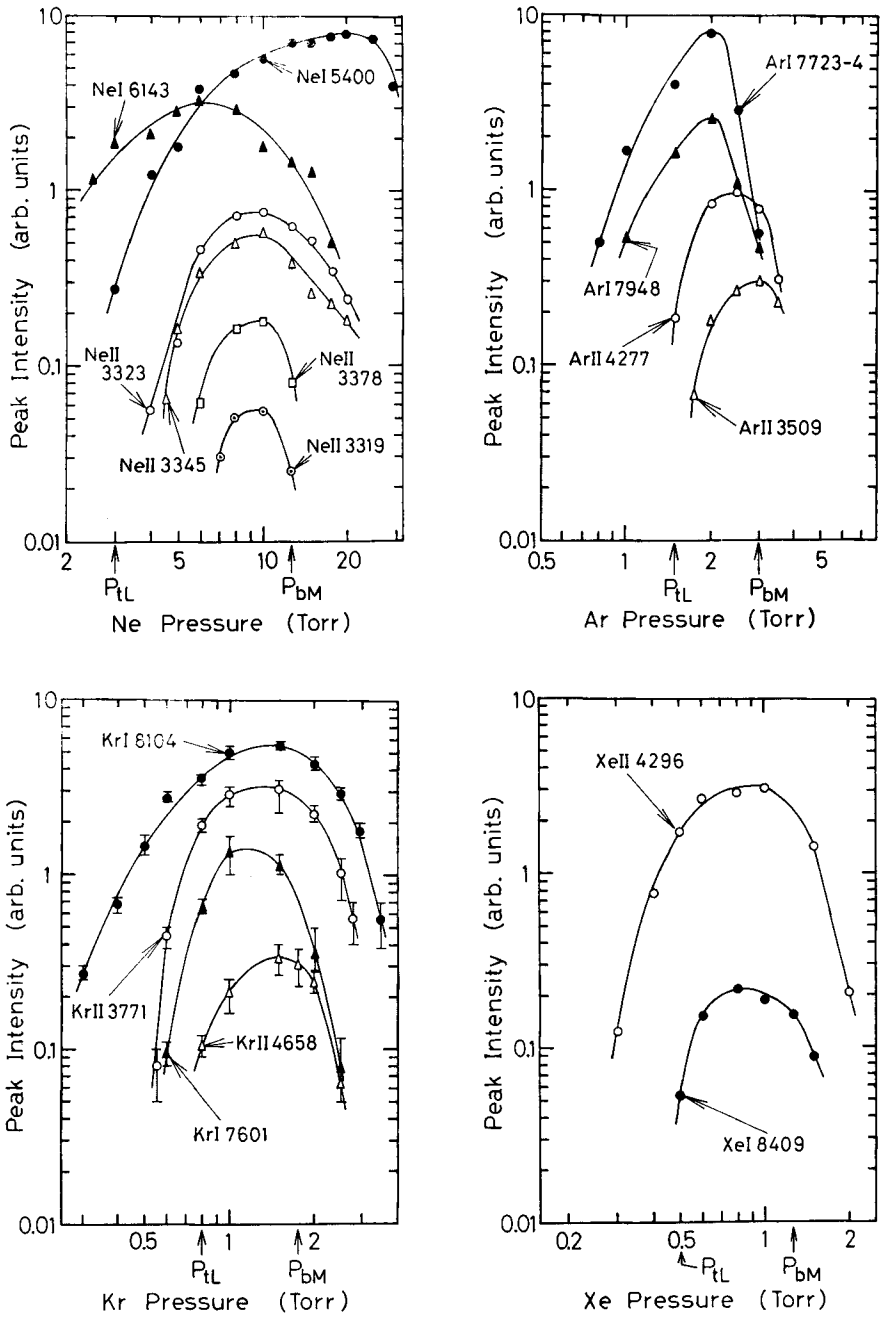

Fig. 4. Pressure dependences of the peak emission intensities of the high-intensity lines for (a) Ne, (b) Ar, (c) Kr, and (d) Xe. The experimenal points are averaged ones over 2~5 shots, and the error bars in (c) indicate the two extremes.

transverse-discharge,[24] and simultaneous discharge.[25-36] The transitions of the singly-ionized lines are as follows: (i) They are ns or $(n-1)d-np$ for Ne, Ar, Kr, and Xe, $np-nd$ for Ar and Kr, and $np-(n+1)s$ for Xe, where $n=3$, 4, 5, and 6 stand for Ne, Ar, Kr, and Xe, respectively. (ii) The transitions of the most intense lines are $ns-np$ for Ne (3323 Å) and Ar (4277 Å), $np-nd$ for Kr (3771 Å), and $np-(n+1)s$ for Xe (4296 Å). (iii) The transitions ns or $(n-1)d-np$ are between doublet levels except for the KrII 4658 Å line. (iv) The transitions $np-nd$ or $(n+1)s$ are between quartet levels, where the upper levels have the total angular momentum J of 1/2. The transitions of the neutral lines are all $ns-np$. Characteristics of the emission behaviors of the high-intensity 17 lines in Table I, except for KrII 4057 and 4475 Å and XeII 4972 Å, were investigated in detail with a spectrograph and with bandpass filters. The four NeII lines and the two ArI lines (7723 and 7724 Å) were not resolved by the bandpass filters.

Figures 4(a), (b), (c), and (d) show the peak emission intensities of the 17 high-intensity spectral lines as a function of pressure for Ne, Ar, Kr, and Xe, respetively. The measurements were carried out with the spectrograph and photodiode at 120 cm from the end window (Fig. 1(a)) for the lines shorter than 7000 Å, and with bandpass filters and the photodiode at 100 cm (Fig. 1(b)) for the lines longer than 7000 Å due to the poor sensitivity of the spectrograph with the photodiode in this region. The pulse form of about 3 ns FWHM as shown in Fig. 3(c), and its appearance time relative to the electron-beam pulse remained almost unchanged at any pressure. In Figs. 4 (a) – (d), the relative intensities are not calibrated among the different lines. The pressures P_{IM} giving the maximum intensity are such that $P_{tL}<P_{IM}<P_{bM}$ for the 17 lines of all the gas species, except for the NeI 5400 Å line which shows $P_{bM}<P_{IM}$. Here, the pressure P_{tL} is that giving the longest duration of the plasma current, and the pressure P_{bM} is that giving the maximum transmission for the electron-beam current density on the drift-tube axis.[1]

Figure 5 shows some typical examples of time-integrated emission patterns of the

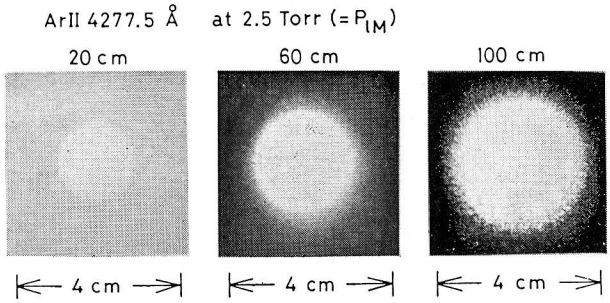

Fig. 5. Time-integrated emission patterns of the high-intensity ArII line at 20, 60, and 100 cm from the end window of 1.4 cm diameter at the pressure P_{IM}.

high-intensity ArII 4277 Å line at 2.5 Torr ($=P_{IM}$), which were photographed in one Febetron shot with a bandpass filter (4272 Å λ_{max} and 75 Å $\Delta\lambda_{1/2}$) on films at 20, 60, and 100 cm from the end window (Fig. 1(b)). These patterns consist of a bright circular area superimposed on a background exposed area spreading over the film. As the distance from the end window increases, the latter fades away, but the former expands with the expansion full angle of about 13 mrad from a point source on the drift-tube axis near the entrance window. Corresponding to the experimental fact of Fig. 3(c), namely that only the high-intensity lines were photographed on the spectrograms without the condensing lens, the bright area is considered to be exposed by the ArII 4277 Å emission, and the background area by spontaneous emissions from the plasma and also probably by the luminescence of the end window bombarded by the electron beam. With increasing or dereasing pressure from P_{IM}, the bright area faded and its contour became vague. The bright area shows a characteristic granular structure as reported so far[31-33,36] for the NeI 5400 and 6143 Å lines. The light emission patterns were similar for the 17 lines, except for NeI 5400 Å. For this line, the contour of the bright circular area was vague at any pressure.

The absolute emission intensities of the high-intensity spectral lines were measured with bandpass filters and the photodiode at 100 cm from the end window (Fig. 1(b)) at the pressures P_{IM}. The bright circular area in Fig. 5 was included within the 3.5 cm diameter photosurface of the photodide. The maximum peak intensities I_{IM} of the 17 lines are given in Table I together with the P_{IM} values in Fig. 4. The values I_{IM} of the four NeII lines were estimated from the relative output of each line of Fig. 4(a) and the total output of the 4 lines with the bandpass filter, assuming that the sum of each output is equal to the total output. The most intense line is KrII 3771 Å with I_{IM} of 240 W for the singly-ionized lines, and KrI 8104 Å with I_{IM} of 440 W for the neutral lines. A calorimeter could not be used for the total energy of μJ, or less, of these lines.

The emission intensity of the high-intensity spectral line was meaured as a function of the plasma length with the bandpass filter and the photodiode at 100 cm from the end window (Fig. 1(c)). Here, the plasma length is the distance between the aluminum foil and the end window, and was varied by moving the foil. The measurements were carried out at the pressure P_{IM} giving the maximum intensity ($>P_{tL}$ as seen in Fig. 4). The foil and its Lucite support scarcely disturbed the electron-beam propagation and the following plasma production. This was confirmed by observing the transmitted beam current with a Faraday cup attached to the drift tube in place of the end window, the azimuthal magnetic field with the magnetic loop coil on the tube wall, and the side-on view of light emission with the open-shutter camera.[1] The plasma was almost uniform along the drift tube above P_{tL}, as shown in the

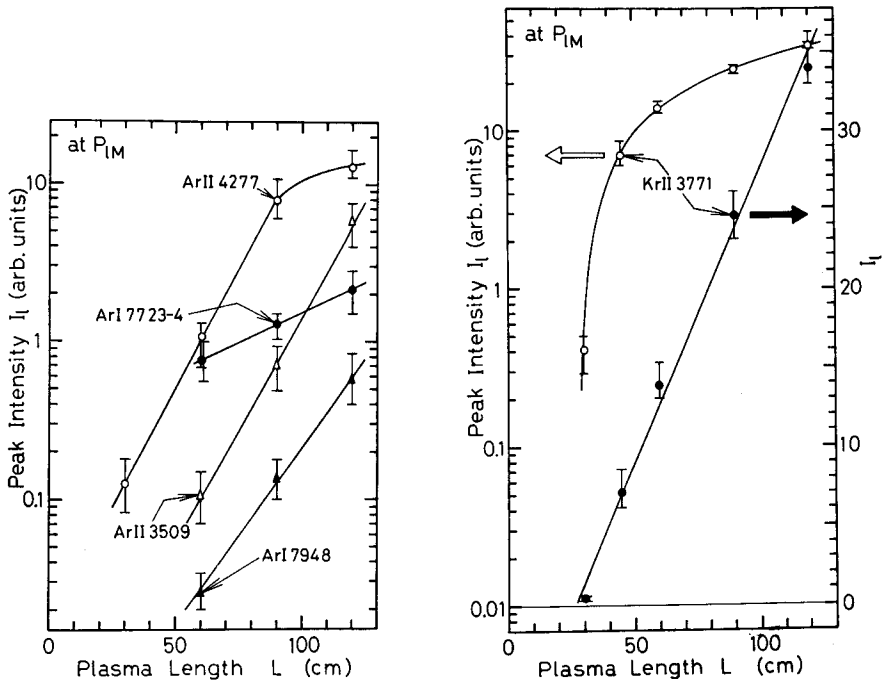

Fig. 6. Peak emission intensities I_l of the high-inensity (a) ArI and II lines and (b), KrII line as a function of plasma length L at the pressures P_{IM}. The experimentl points are averaged ones over 5~10 shots, and the error bars indicate the two extremes.

experiments of the previous paper.[1] The plasma condition remained almost unchanged for the movement of the aluminum foil. At any foil position, a pulse form of about 3 ns FWHM was observed for the high-intensity line as shown in Fig. 3(c), and its appearance time remained almost unchaged.

Figure 6(a) shows the peak emission intensities I_l of the high-intensity spectral lines as a function of the plasma length L for Ar. The data exhibit exponential behaviors $I_l \propto e^{\alpha L}$, and therefore, α is regarded as a small signal gain coefficient. For Ne, Kr, and Xe, the high-intensity lines also exhibited the exponential increment, except for KrII 3771 and 4658 Å, XeII 4296 Å, and KrI 8104 Å. These four lines exhibited the linear behavior $I_l \propto \beta L$ with a constant β as shown for KrII 3771 Å in Fig. 6(b). The linear increment means the saturation behavior as reported so far for the N_2 3371 Å[37] and CH_3F 496 μm[38] lasers. In Table I, the values α are given for the lines exhibiting the exponential behavior, and the designations Sat. for the lines exhibiting the linear behavior. In Figs. 6(a) and (b), the relative intensities are not calibrated among the different lines, and the values of I_l at $L=120$ cm correspond to the I_{IM} values in Table I.

The short-pulsed and intense emissions of the singly-ionized and neutral atomic lines in Table I, which arrive at the end of the drift tube almost simultaneosly with the electron-beam pulse, are highly directional, as shown in Figs. 3(b) and 5. Their amplification processes are evident in Fig. 6. Therefore, these emissions are regarded as self-terminating lasers traveling along with the electron beam as suggested in ref. 39. Investigations of their spatial and temporal coherences[29,31-33,36] are now in progress.

3. 2 Side-on observation

Figure 7 shows some typical examples of oscilloscope traces of the side-on emissions of the ArII 4277 Å ($4s'^2D_{5/2}-4p'^2P^o_{3/2}$) laser line and the ArII 4348 Å ($4s^4P_{5/2}-4p^4D^o_{7/2}$) spontaneous line. The measurements were performed with the spectrograph and photomultiplier (Fig. 1(a)) at several Ar pressures. These signals first consist of a short pulse, and then a succeeding long one. The former appears at any pressure, and is due to an X-ray emission (Bremsstrahlung by the high-energy beam electrons at the drift-tube wall) which enters the photomultiplier due to incomplete X-ray shielding. The latter appears above 0.4 Torr, and is due to the light emission from the plasma induced by the electron beam.[1] A time interval of about 15 ns between the rises of the X-ray and light pulses is attributable to the difference of about 450 cm between the X-ray and light paths from their sources to the photomultiplier. The greatest part of this difference is the optical path in the spectrograph. Accordingly, the light emission is considered to appear at almost the same time as the arrival of the

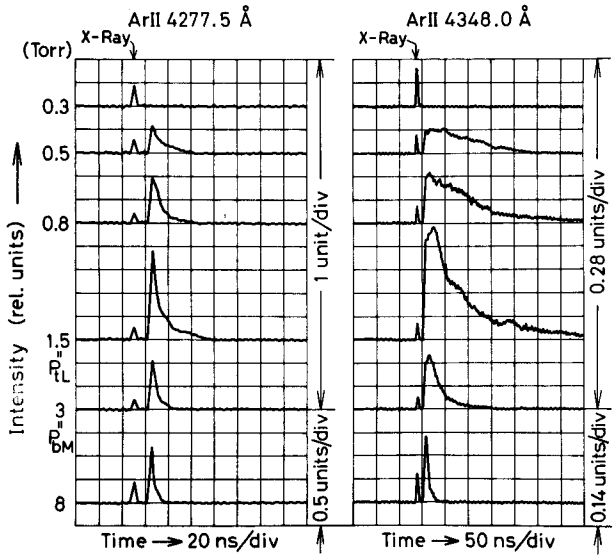

Fig. 7. Oscilloscope traces of the side-on emissions of the two ArII lines at several Ar pressures.

electron-beam pulse at the viewing point, i. e., 58 cm from the entrance window.

As seen in Fig. 7, the side-on emission intensities of the ArII 4277 and 4348 Å lines rise in a few nanoseconds, and then the former decays fast but the latter still rises slightly until its slow decay. As the pressure is increased, the peak intensities and durations of the emissions of both lines increase to their maxima at 1.5 Torr and then decrease. The pressure $(P_{IM})_{side\text{-}on}$ giving these intensity maxima is equal to the pressure P_{tL} giving the longest duration of the plasma current.[1] The pressure $P_{IM}=(P_{IM})_{end\text{-}on}$ giving the intensity maximum in the end-on observation was also equal to P_{tL} for the spontaneous line, although $P_{IM}>P_{tL}$ for the laser line, as seen in Fig. 4. With any further increase of pressure above P_{tL}, the emission durations become short and the decay times become near the radiative lifetimes τ of the upper levels of the transitions concerned ($\tau=5.54$ and 5.64 ns[40] for ArII $4p'^2P^o_{3/2}$ and $4p^4D^o_{7/2}$, respectively). This corresponds to the shortening of the duration of the plasma current, as shown in the previous paper.[1] The behaviors of side- and end-on emissions of the laser lines and many other spontaneous lines were almost the same for NeII, ArII, KrII, and XeII with $P_{tL}=3$, 1.5, 0.8, and 0.5 Torr, respectively.

The observed spectral lines of NeII, ArII, KrII, and XeII are listed in Table II(a), (b), (c), and (d). respectively, The upper levels of these transitions have the configurations of np, np', np'', nd, and $(n+1)s$ with $n=3$, 4, 5, and 6 for Ne, Ar, Kr, and Xe, respectively. Their energies E_j are measured from the neutral-atom ground level. Here no-, single-, and double-primes stand for the ^3P, ^1D, and ^1S cores, respectively. In this table are also given the relative peak intensities I_{jk} and the durations t_{dur} of the emissions at the pressures P_{tL}. Here, the peak intensity means the initial fast rise for the lines showing the second peak of the slow rise (*e. g.*, ArII 4348 Å in Fig. 7), and the duration means the time of FWHM. The emissions of these lines show various durations t_{dur} between 5 and 120 ns. For the laser lines (also see Table I), the intensities I_{jk} are large, and the durations t_{dur} are short, i. e., between 5 and 12 ns, except for KrII 4658 Å ($t_{dur}=40$ ns). In the course of the measurements of I_{jk} and t_{dur} from shot to shot of the Febetron, the ArII 4277 Å emission was monitored every 20 shots to check the unchangeability of the optical system.

Table II also includes the radiative transition probabilities A_{jk} and the relative population densities n_j of the upper levels of the transitions concerned, where $n_j=I_{jk}\lambda/A_{jk}hc$ on the assumption that the plasma is optically thin in the direction of the side-on view. Here, c is the velocity of light and h is Planck's constant. The values A_{jk} of the NeII lines are given by Wiese *et al.*,[41] except for the lines from 4s levels. The values of the lines from 4s levels are given by Loginov *et al.*[42] The values A_{jk} of the ArII lines are given by Wiese *et al.*[43] In contrast to a fair agreement between the various values of A_{jk} so far reported for the NeII and ArII lines, those for the KrII

Table II(a). Spectral lines of NeII observed in the direction of side-on view.

Transition (Lower—Upper)	λ (Å)	E_j (eV)	I_{jk}* (rel.)	A_{jk} ($10^8 s^{-1}$)	n_j (rel.)	t_{dur}* (ns)	Refs.
$3s^2P_{3/2} - 3p^2S^o_{1/2}$	3481.9	52.90	1.4	1.2	4.1	14	47, 48
$3s^2P_{1/2} - 3p^2P^o_{1/2}$	3378.2[a]	53.09	5.0	1.3	13	9.0	47, 48
$3s^2P_{3/2} - 3p^2P^o_{3/2}$	3323.7[b]	53.07	8.5	1.4	20	8.8	47, 48
$3s^2P_{1/2} - 3p^2D^o_{3/2}$	3727.0	52.74	2.8	1.0	10	19	47, 48
$3s^2P_{3/2} - 3p^2D^o_{5/2}$	3713.0	52.68	4.1	1.3	12	11	48
$3s^4P_{3/2} - 3p^4S^o_{3/2}$	3001.6	52.92	~0	0.78	—	—	48
$3s^4P_{3/2} - 3p^4P^o_{1/2}$	3709.6	52.13	~0	1.1	—	—	48
$3s^4P_{5/2} - 3p^4P^o_{3/2}$	3664.1	52.11	0.80	0.67	4.4	23	48
$3s^4P_{5/2} - 3p^4P^o_{5/2}$	3694.1	52.08	1.6	0.96	6.2	23	48
$3s^4P_{3/2} - 3p^4D^o_{1/2}$	3311.3[c]	52.53	0.15	0.30	1.7	25	48
$3s^4P_{3/2} - 3p^4D^o_{3/2}$	3327.1	52.52	0.42	0.98	1.4	20	47, 48
$3s^4P_{5/2} - 3p^4D^o_{5/2}$	3297.7	52.49	0.39	0.53	2.4	11	48
$3s^4P_{5/2} - 3p^4D^o_{7/2}$	3334.8	52.44	1.0	1.8	1.9	21	48
$3s'^2D_{3/2} - 3p'^2P^o_{1/2}$	3319.7[d]	55.84	3.9	1.7	7.6	7.0	48
$3s'^2D_{5/2} - 3p'^2P^o_{3/2}$	3345.4[e]	55.81	8.6	1.5	19	9.5	48
$3s'^2D_{3/2} - 3p'^2D^o_{3/2}$	3232.3[f]	55.94	1.6	1.7	3.0	8.5	48
$3s'^2D_{5/2} - 3p'^2D^o_{5/2}$	3230.1[g]	55.94	0.62	1.8	1.1	8.0	48
$3s'^2D_{3/2} - 3p'^2F^o_{5/2}$	3574.6[h]	55.58	2.4	1.3	6.6	10	48
$3s'^2D_{5/2} - 3p'^2F^o_{7/2}$	3568.5	55.58	3.6	1.3	9.9	11	48
$3s''^2S_{1/2} - 3p''^2P^o_{1/2}$	3479.5	59.42	0.91	1.6	2.0	8.5	48
$3s''^2S_{1/2} - 3p''^2P^o_{3/2}$	3480.7	59.42	2.5	1.6	5.4	9.7	48
$3p^2S^o_{1/2} - 3d^2P_{1/2}$	3503.6	56.44	0.43	1.9	0.79	10	48
$3p^2S^o_{1/2} - 3d^2P_{3/2}$	3456.6[i]	56.49	0.30	1.0	1.0	10	48
$3p^2P^o_{1/2} - 3d^2D_{3/2}$	3818.4	56.33	0.27	0.69	1.5	13	48
$3p^2P^o_{3/2} - 3d^2D_{5/2}$	3829.7	56.31	0.83	0.88	3.6	11	48
$3p^2D^o_{3/2} - 3d^2F_{5/2}$	3414.8	56.37	0.29	0.41	2.4	10	48
$3p^2D^o_{5/2} - 3d^2F_{7/2}$	3417.7[j]	56.31	0.69	2.0	1.2	13	48
$3p^4S^o_{3/2} - 3d^4P_{1/2}$	3594.1	56.37	~0	1.3	—	—	48
$3p^4S^o_{3/2} - 3d^4P_{3/2}$	3565.8	56.40	~0	0.82	—	—	48
$3p^4S^o_{3/2} - 3d^4P_{5/2}$	3542.9[k]	56.42	~0	1.3	—	—	48
$3p^4P^o_{1/2} - 3d^4D_{1/2}$	3045.5	56.20	~0	2.5	—	—	
$3p^4P^o_{1/2} - 3d^4D_{3/2}$	3054.6	56.19	~0	0.93	—	—	48
$3p^4P^o_{3/2} - 3d^4D_{5/2}$	3047.5	56.18	~0	1.8	—	—	48
$3p^4P^o_{5/2} - 3d^4D_{7/2}$	3034.4	56.17	~0	3.1	—	—	48
$3p^4D^o_{1/2} - 3d^4F_{3/2}$	3213.7[l]	56.39	0.46	1.8	0.82	8.5	48
$3p^4D^o_{3/2} - 3d^4F_{5/2}$	3190.8	56.40	~0	0.73	—	—	48
$3p^4D^o_{5/2} - 3d^4F_{7/2}$	3198.6	56.36	~0	2.2	—	—	48
$3p^4D^o_{7/2} - 3d^4F_{9/2}$	3218.2	56.30	0.23	3.6	0.21	14	48

$3p^2D^o_{3/2}-4s^2P_{1/2}$	3088.2	56.76	0.18	1.51	0.37	13	
$3p^2P^o_{3/2}-4s^2P_{3/2}$	3428.7	56.69	0.44			13	48
$3p^4D^o_{1/2}-4s^4P_{1/2}$	3044.1	56.61	~0	0.93	—	—	48
$3p^4D^o_{3/2}-4s^4P_{3/2}$	3059.1	56.57	~0	0.53	—	—	48
$3p^4D^o_{7/2}-4s^4P_{5/2}$	3039.6	56.52	~0	1.47	—	—	48

* Averaged value over 2~5 shots at 3 Torr ($=P_{tL}$).

[a,b,d,e] Observed laser lines in Table I.

[c-1] Spectral resolution of photoelectric observation with the spectrograph was more or less 0.5 Å; accordingly these lines were blended with the nearby NeII lines as seen in Striganov's table,[21] and the n_{jk} values need some corrections.

Table II(b). Spectral lines of ArII observed in the direction of side-on view.

Transition (Lower—Upper)	λ (Å)	E_j (eV)	I_{jk}* (rel.)	A_{jk} ($10^8 s^{-1}$)	n_j (rel.)	t_{dur}* (ns)	Refs.
$4s^2P_{1/2}-4p^2S^o_{1/2}$	4579.3	35.72	3.8	0.82	21	12	46, 49, 50, 51, 52
$4s^2P_{3/2}-4p^2P^o_{1/2}$	4657.8	35.55	5.6	0.81	32	13	46, 49, 50, 51, 52
$4s^2P_{3/2}-4p^2P^o_{3/2}$	4545.0	35.62	6.5	0.41	72	13	46, 50
$4s^2P_{1/2}-4p^2D^o_{3/2}$	4965.0	35.51	3.3	0.34	48	14	46, 49, 50, 51, 52
$4s^2P_{3/2}-4p^2D^o_{5/2}$	4879.8	35.43	4.9	0.78	31	28	49, 50, 51, 52
$4s^4P_{3/2}-4p^4S^o_{3/2}$	3850.5	35.72	1.5	0.47	12	40	46, 51
$4s^4P_{3/2}-4p^4P^o_{1/2}$	4847.8	35.05	1.9	0.85	11	24	46
$4s^4P_{5/2}-4p^4P^o_{3/2}$	4735.9	35.01	2.4	0.58	20	28	46, 50
$4s^4P_{5/2}-4p^4P^o_{5/2}$	4806.0	34.97	3.3	0.79	20	28	50, 51
$4s^4P_{1/2}-4p^4D^o_{1/2}$	4379.6[a]	35.39	2.4	1.04	10	26	46, 50
$4s^4P_{1/2}-4p^4D^o_{3/2}$	4430.1[b]	35.36	2.3	0.53	19	20	46, 50
$4s^4P_{3/2}-4p^4D^o_{5/2}$	4426.0	35.30	3.7	0.83	20	33	50, 51
$4s^4P_{5/2}-4p^4D^o_{7/2}$	4348.0	35.24	3.7	1.24	13	43	50
$4s'^2D_{3/2}-4p'^2P^o_{1/2}$	4131.7	37.18	6.2	1.4	18	6.0	46, 50
$4s'^2D_{5/2}-4p'^2P^o_{3/2}$	4277.5[c]	37.10	11	1.0	47	6.6	46, 50
$4s'^2D_{3/2}-4p'^2D^o_{3/2}$	4042.8[d]	37.24	2.0	1.4	5.8	16	46
$4s'^2D_{5/2}-4p'^2D^o_{5/2}$	4072.0[e]	37.25	4.3	0.57	31	19	
$4s'^2D_{3/2}-4p'^2F^o_{5/2}$	4589.8	36.88	3.5	0.82	20	18	50
$4s'^2D_{5/2}-4p'^2F^o_{7/2}$	4609.5	36.89	5.4	0.91	27	18	50
$4s''^2S_{1/2}-4p''^2P^o_{1/2}$	3994.7[f]	39.60	0.94	1.6	2.3	6.1	
$4s''^2S_{1/2}-4p''^2P^o_{3/2}$	4052.9[g]	39.55	1.8	1.5	4.9	6.0	
$4p^2P^o_{1/2}-4d^2P_{1/2}$	3307.2[h]	39.30	0.90	3.4	0.88	9.0	
$4p^2S^o_{1/2}-4d^2P_{3/2}$	3388.5	39.38	1.2	1.9	2.1	9.0	
$4p^2P^o_{1/2}-4d^2D_{3/2}$	3028.9[i]	39.64	0.10	2.3	0.13	5.0	
$4p^2P^o_{3/2}-4d^2D_{5/2}$	3093.4	39.62	0.37	4.4	0.26	9.5	
$4p^2D^o_{3/2}-4d^2F_{5/2}$	3545.5[j]	39.01	3.5	3.4	3.6	13	
$4p^2D^o_{5/2}-4d^2F_{7/2}$	3559.5	38.91	2.7	3.9	2.5	14	
$4p^4S^o_{3/2}-4d^4P_{1/2}$	3979.3	38.83	1.0	1.3	3.1	11	

Transition (Lower—Upper)	λ (Å)	E_j (eV)	I_{jk}* (rel.)	A_{jk} ($10^8 s^{-1}$)	n_j (rel.)	t_{dur}* (ns)	Refs.
$4p^4S^o_{3/2} - 4d^4P_{3/2}$	3932.5[k]	38.87	1.2	1.1	4.3	18	
$4p^4S^o_{3/2} - 4d^4P_{5/2}$	3868.5	38.92	1.7	1.9	3.5	13	
$4p^4P^o_{1/2} - 4d^4D_{1/2}$	3509.7[l]	38.59	3.7	2.5	5.2	5.0	
$4p^4P^o_{1/2} - 4d^4D_{3/2}$	3535.3	38.56	1.2	0.82	5.2	16	
$4p^4P^o_{3/2} - 4d^4D_{5/2}$	3514.3	38.54	0.91	1.23	2.6	11	
$4p^4P^o_{5/2} - 4d^4D_{7/2}$	3491.5[m]	38.52	2.7	3.0	3.1	15	
$4p^4D^o_{1/2} - 4d^4F_{3/2}$	3581.6[n]	38.85	2.6	1.8	5.2	10	
$4p^4D^o_{3/2} - 4d^4F_{5/2}$	3582.3[o]	38.82	3.7	3.72	3.6	11	
$4p^4D^o_{5/2} - 4d^4F_{7/2}$	3576.6[p]	38.76	3.3	2.77	4.3	32	
$4p^4D^o_{7/2} - 4d^4F_{9/2}$	3588.4	38.70	3.5	3.39	3.7	17	
$4p^2P^o_{3/2} - 5s^2P_{1/2}$	4222.6	38.55	1.1	0.69	6.7	9.2	51
$4p^2P^o_{1/2} - 5s^2P_{3/2}$	4275.1	38.45	0.55	0.26	9.0	23	
$4p^4D^o_{3/2} - 5s^4P_{1/2}$	4033.8	38.43	0.90	0.98	3.7	15	
$4p^4D^o_{3/2} - 5s^4P_{3/2}$	4156.0	38.34	0.67	0.39	7.1	13	
$4p^4D^o_{5/2} - 5s^4P_{5/2}$	4179.3[q]	38.26	0.22	0.13	7.1	7.5	

* Averaged value over 2~5 shots at 1.5 Torr ($=P_{tL}$).

[c,l] Observed laser lines in Table I.

[a,b,d-k,m-q] These lines were blended with the nearby ArII lines[21] (see the footnote of Table II (a)).

Table II(c). Spectral lines of KrII observed in the direction of side-on view.

Transition (Lower—Upper)	λ (Å)	E_j (eV)	I_{jk}* (rel.)	A_{jk} ($10^8 s^{-1}$)	n_j (rel.)	t_{dur}* (ns)	Refs.
$5s^2P_{1/2} - 5p^2S^o_{1/2}$	4680.4[a]	31.64	2.5	1.66	7.0	16	47, 53, 54
$5s^2P_{3/2} - 5p^2P^o_{1/2}$	4846.6	31.24	3.5	1.75	9.7	21	47, 53, 54
$5s^2P_{3/2} - 5p^2P^o_{3/2}$	4615.2[b]	31.36	3.2	0.87	17	21	47, 53, 54
$5s^2P_{1/2} - 5p^2D^o_{3/2}$	4762.4	31.59	3.8	0.78	23	22	47
$5s^2P_{3/2} - 5p^2D^o_{5/2}$	4619.1[c]	31.36	3.0	1.47	9.4	50	53, 54
$5s^4P_{1/2} - 5p^4S^o_{3/2}$	4145.1	31.56	1.1	0.38	12	29	54
$5s^4P_{3/2} - 5p^4P^o_{1/2}$	4832.0	30.82	4.0	1.46	13	23	53, 54
$5s^4P_{5/2} - 5p^4P^o_{3/2}$	4658.8[d]	30.64	4.3	1.12	18	40	53, 54
$5s^4P_{5/2} - 5p^4P^o_{5/2}$	4739.0	30.59	4.7	1.50	15	65	53, 54
$5s^4P_{1/2} - 5p^4D^o_{1/2}$	4431.6	31.37	2.9	1.14	11	33	53, 54
$5s^4P_{3/2} - 5p^4D^o_{3/2}$	4292.9	31.15	7.2	0.67	46	18	47, 53, 54
$5s^4P_{3/2} - 5p^4D^o_{5/2}$	4765.7	30.86	4.4	1.21	17	58	53, 54
$5s^4P_{5/2} - 5p^4D^o_{7/2}$	4355.4	30.82	5.0	1.00	22	70	54
$5s'^2D_{3/2} - 5p'^2P^o_{1/2}$	4057.0[e]	32.86	8.4	0.78	44	7.0	54
$5s'^2D_{5/2} - 5p'^2P^o_{3/2}$	4475.0[f]	32.61	9.5	1.12	38	7.5	53, 54
$5s'^2D_{3/2} - 5p'^2D^o_{3/2}$	4065.1[g]	32.86	4.5	0.63	29	15	54
$5s'^2D_{5/2} - 5p'^2D^o_{5/2}$	4088.3	32.87	4.9	0.84	24	20	54

$5s'^2D_{3/2}-5p'^2F^o_{5/2}$	4633.8	32.48	4.4	1.24	16	35	53, 54
$5s'^2D_{5/2}-5p'^2F^o_{7/2}$	4577.2	32.55	1.3	1.54	3.9	43	53, 54
$5s''^2S_{1/2}-5p''^2P^o_{1/2}$	4453.2	34.85	1.2	1.53	3.5	11	54
$5s''^2S_{1/2}-5p''^2P^o_{3/2}$	4322.9	34.93	3.2	1.66	8.3	12	54
$5p^2P^o_{1/2}-5d^2P_{1/2}$	3589.6	34.69	1.5			8.0	
$5p^4D^o_{3/2}-5d^2P_{3/2}$	3735.7	34.46	1.5			8.5	
$5p^2D^o_{3/2}-5d^2D_{3/2}$	3857.3	34.81	0.48			9.5	
$5p^2D^o_{3/2}-5d^2D_{5/2}$	3607.8	35.03	2.8			11	54
$5p^4S^o_{3/2}-5d^2F_{5/2}$	3875.4	34.76	0.85			16	
$5p'^2D^o_{5/2}-5d^2F_{7/2}$	3906.2	36.05	1.1			16	
$5p^4P^o_{3/2}-5d^4P_{1/2}$	3771.3[b]	33.93	5.3			6.5	54
$5p^4P^o_{3/2}-5d^4P_{3/2}$	3686.1	34.00	2.3			12	
$5p^4P^o_{5/2}-5d^4P_{5/2}$	3690.6	33.95	0.27			18	
$5p^4D^o_{1/2}-5d^4D_{1/2}$	4371.2	34.20	0.69			9.2	
$5p^4D^o_{3/2}-5d^4D_{3/2}$	4268.5[i]	34.05	0.90			7.0	54
$5p^4P^o_{5/2}-5d^4D_{5/2}$	3631.8	34.01	1.8			11	54
$5p^4P^o_{5/2}-5d^4D_{7/2}$	3653.9	33.99	1.6			31	
$5p^4D^o_{1/2}-5d^4F_{3/2}$	3718.6[j]	34.70	3.2			15	54
$5p^4D^o_{3/2}-5d^4F_{5/2}$	3744.8	34.46	1.9			18	54
$5p^4D^o_{5/2}-5d^4F_{7/2}$	3778.0	34.14	1.7			23	54
$5p^4D^o_{7/2}-5d^4F_{9/2}$	3783.1	34.10	2.1			31	54
$5p^4S^o_{3/2}-6s^2P_{1/2}$	4796.3	34.14	0.37			9.0	
$5p^2D^o_{5/2}-6s^2P_{3/2}$	4556.6	34.08	0.58			10	54
$5p^4P^o_{3/2}-6s^4P_{1/2}$	3623.6	34.06	0.93			7.5	
$5p^4P^o_{1/2}-6s^4P_{3/2}$	4523.1	33.56	0.40			17	
$5p^4P^o_{5/2}-6s^4P_{5/2}$	4317.8	33.46	1.6			29	54

* Averaged value over 2～5 shots at 0.8 Torr ($=P_{tL}$).

[d-f,h] Observed laser lines in Table I.

[a-c,g,i,j] These lines were blended with the nearby KrII lines[21] (see the footnote of Table II(a)).

Table II(d). Spectral lines of XeII observed in the direction of side-on view.

Transition (Lower—Upper)	λ (Å)	E_j (eV)	I_{jk}* (rel.)	A_{jk} ($10^8 s^{-1}$)	n_j (rel.)	t_{dur}* (ns)	Refs.
$6s^2P_{3/2}-6p^2S^o_{1/2}$	5438.9	27.14	2.7	3.76	3.9	27	55
$6s^2P_{1/2}-6p^2P^o_{1/2}$	4919.6	27.56	1.5	0.74	10	17	
$6s^2P_{3/2}-6p^2P^o_{3/2}$	4887.3	27.40	2.1	0.42	24	20	
$6s^2P_{1/2}-6p^2D^o_{3/2}$	4988.7	27.53	0.84	0.35	12	53	55
$6s^2P_{3/2}-6p^2D^o_{5/2}$	4921.4	27.38	3.5	1.23	14	78	55
$6s^4P_{1/2}-6p^4S^o_{3/2}$	4883.5[a]	27.20	2.5	0.77	16	51	55, 56
$6s^4P_{3/2}-6p^4P^o_{1/2}$	5372.3	26.21	3.3	2.76	6.4	24	55
$6s^4P_{5/2}-6p^4P^o_{3/2}$	5339.3[b]	25.98	2.8	1.88	8.0	54	55

Transition (Lower—Upper)	λ (Å)	E_j (eV)	I_{jk}* (rel.)	A_{jk} ($10^8 s^{-1}$)	n_j (rel.)	t_{dur}* (ns)	Refs.
$6s^4P_{5/2} - 6p^4P^o_{5/2}$	5292.2[e]	26.01	4.9	2.32	11	80	55, 56
$6s^4P_{1/2} - 6p^4D^o_{1/2}$	5191.3[d]	27.05	1.7	3.2	2.8	35	55
$6s^4P_{3/2} - 6p^4D^o_{3/2}$	4603.0	26.60	8.2	0.69	55	15	55, 56
$6s^4P_{5/2} - 6p^4D^o_{5/2}$	4890.0	26.19	1.2	0.10	59	58	
$6s^4P_{5/2} - 6p^4D^o_{7/2}$	4844.3	26.22	2.8	0.77	18	120	55
$6s'^2D_{3/2} - 6p'^2P^o_{1/2}$	5044.9	28.58	3.0			9.7	55
$6s'^2D_{5/2} - 6p'^2P^o_{3/2}$	4615.5[e]	28.20	1.5	0.47	15	14	55, 56
$6s'^2D_{3/2} - 6p'^2D^o_{3/2}$	5261.9	28.48	2.0	5.43	1.9	27	55
$6s'^2D_{3/2} - 6p'^2D^o_{5/2}$	5184.4	28.51	0.52	1.23	2.2	30	
$5d^2D_{3/2} - 6p'^2F^o_{5/2}$	4769.0	28.10	0.91	0.20	22	19	55, 56
$5d^2D_{5/2} - 6p'^2F^o_{7/2}$	4876.5	28.24	3.1	0.94	16	32	
$\cdots - 6p''^2P^o_{1/2}$							
$6s''^2S_{1/2} - 6p''^2P^o_{3/2}$	6194.0	29.50	~0		—	—	
$6p^2S^o_{1/2} - 6d^2P_{1/2}$	4158.0	30.12	0.67	0.27	10	12	
$\cdots - 6d^2P_{3/2}$							
$6p^2P^o_{3/2} - 6d^2D_{3/2}$	4406.8	30.21	0.54	0.62	3.8	14	
$6p^2P^o_{3/2} - 6d^2D_{5/2}$	4731.1	30.02	0.21	3.7	0.27	16	
$\cdots - 6d^2F_{5/2}$							
$\cdots - 6d^2F_{7/2}$							
$6p^4S^o_{3/2} - 6d^4P_{1/2}$	5192.1[f]	29.59	0.48			18	
$6p^4S^o_{3/2} - 6d^4P_{3/2}$	4440.9	29.99	0.23	0.47	2.2	36	
$6p^4S^o_{3/2} - 6d^4P_{5/2}$	4592.0	29.90	0.60	0.89	3.1	21	
$\cdots - 6d^4D_{1/2}$							
$6p^4P^o_{3/2} - 6d^4D_{3/2}$	4180.1	28.94	1.9	0.42	19	18	55, 56
$6p^4P^o_{5/2} - 6d^4D_{5/2}$	4238.2	28.92	1.7	0.91	7.9	30	
$6p^4P^o_{5/2} - 6d^4D_{7/2}$	4245.3[g]	28.92	2.4	0.74	14	35	55
$6p^4D^o_{3/2} - 6d^4F_{3/2}$	4373.7	29.43	1.2	0.32	16	6.5	
$6p^4D^o_{3/2} - 6d^4F_{5/2}$	4480.8	29.36	2.3	1.33	7.7	10	55
$6p^4D^o_{5/2} - 6d^4F_{7/2}$	4330.5	29.05	2.4	1.29	8.1	50	55
$\cdots - 6d^4F_{9/2}$							
$6p^2P^o_{1/2} - 7s^2P_{1/2}$	5445.5	29.84	0.47			5.5	
$6p^2D^o_{5/2} - 7s^2P_{3/2}$	5188.1	29.77	0.91	4.9	0.96	15	55
$6p^4P^o_{3/2} - 7s^4P_{1/2}$	4296.4[h]	28.86	4.7	0.72	28	7.2	55
$6p^4P^o_{1/2} - 7s^4P_{3/2}$	5122.4	28.63	0.83	0.05	85	15	
$6p^4P^o_{5/2} - 7s^4P_{5/2}$	4862.5	28.55	1.2	0.72	8.1	30	

* Averaged value over 2~5 shots at 0.5 Torr ($=P_{tL}$).

[h] Observed laser line in Table I. Another laser line 4972.7 Å ($5d^2D_{5/2} - 6p'^2P^o_{3/2}$, $E_j = 28.20$), having the same upper level as 4615.5' Å in this table, showed $I_{jk} = 3.7$ ($A_{jk} = 0.96$, $n_j = 19$) and $t_{dur} = 12$ ns.

[a–h] These lines were blended with the nearby XeII lines[21] (see the footnote of Table II(a)).

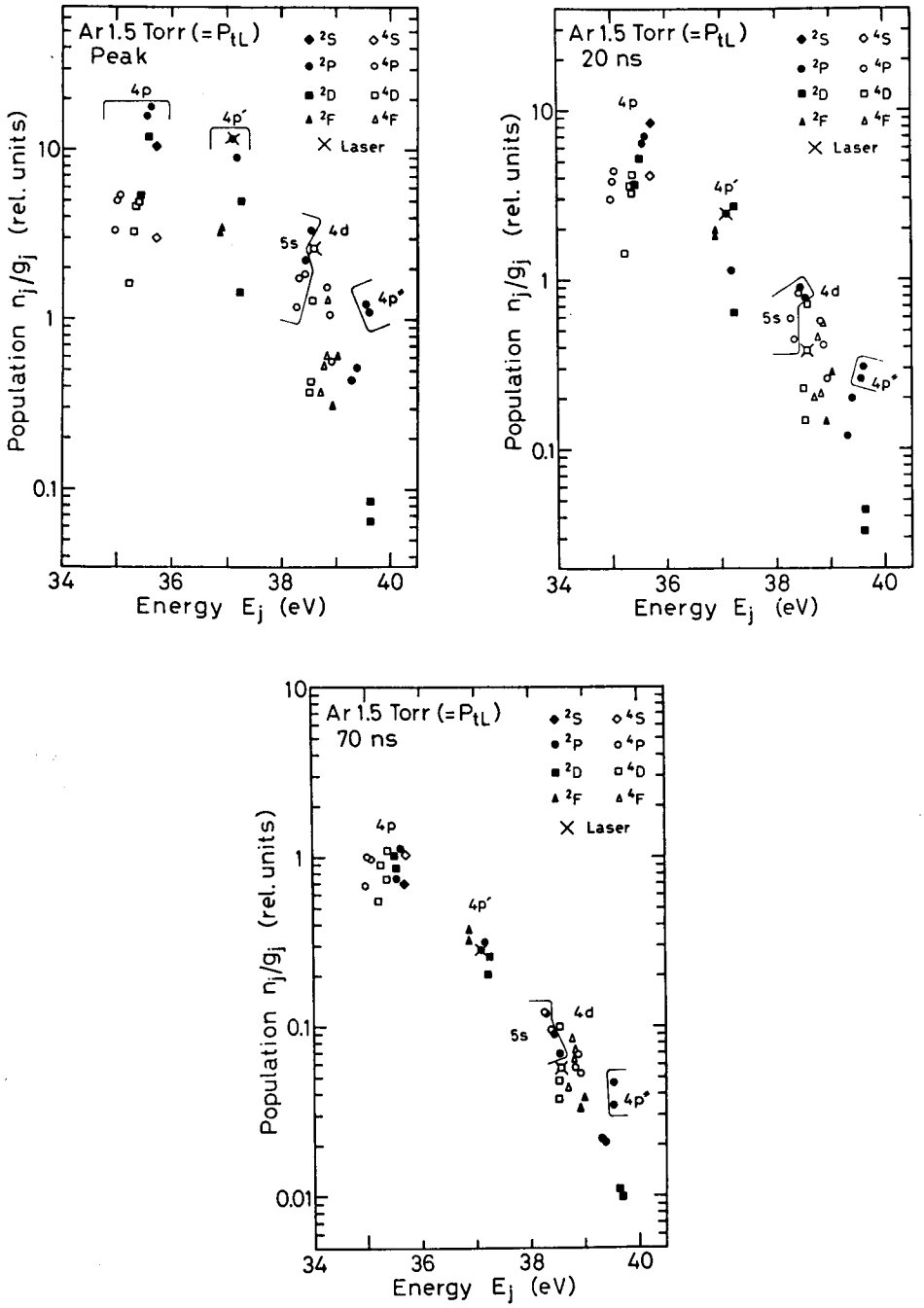

Fig. 8. Population densities n_j of the ArII levels divided by their degeneracies g_j at (a) the peak, (b) 20, and (c) 70 ns, using the data at the pressure P_{tL}. The experimental points are averaged ones over 2~5 shots.

and XeII lines are not in agreement. Here, the values A_{jk} of the KrII and XeII lines are those given by Spector *et al.*[44] and by Miller *et al.*,[45] respectively. The emission of the HeII 4685.6 Å line ($3d^2D-4f^2F^o$ and $E_j=75.59$ eV), which was the only HeII line observed, showed I_{jk} of 2.1 and t_{dur} of 6.0 ns at P_{tL} ($=10$ Torr$=(P_{1M})_{side\text{-}on}$).

Figures 8 (a), (b), and (c) show the relative population densities n_j of the ArII levels divided by their degeneracies g_j at the peak of the initial fast rise, 20, and 70 ns, respectively, using the data of the side-on emissions of the ArII lines in Table II(b) at P_{tL} ($=1.5$ Torr).

§ 4. Discussion

Simultaneous ionization and excitation from a neutral-atom ground level by energetic-electron impact is a dominant process in populating upper levels of singly-ionized ion lasers in fast pulsed discharge. As indicated in the Refs. in Table II, the theoretical[46,47] and experimental[48-56] cross sections have been obtained for NeII, ArII, KrII, and XeII.

The optical cross section Q_{jk} is estimated as a function of electron energy E_e from the emission intensity I_{jk} of the $j\rightarrow k$ transition due to the simultaneous ionization and excitation from the neutral ground level by electron impact:[48-56]

$$\frac{I_{jk}\lambda}{hc}=A_{jk}n_j\equiv Q_{jk}v_e n_e n_g. \qquad (1)$$

Here n_j, n_e, and n_g are the densities of the j-level, electron, and neutral gas, respectively, and v_e is the electron velocity. Figure 9 shows some typical examples of the cross sections Q_{jk} as a function of E_e for the several NeII,[48] ArII,[50] and KrII[54] lines in Table II. The absolute values Q_0 at their maxima are also indicated in this figure. The upper levels of these transitions belong to the np′ and np configurations with $n=3$, 4, and 5 for Ne, Ar, and Kr, respectively. The lines with the np′ configuration are the laser lines in Table I. The uppermost functions $Q_{jk}(E_e)$ are much broader than the lower three. Among these lower three, the functions $Q_{jk}(E_e)$ with a larger J-value are more peaked and exhibit more resonant shapes near the threshold energies E_{eT} ($=E_j$ in Table II). The laser lines generally have broad functions $Q_{jk}(E_e)$, except for KrII 3771 and 4658 Å.

The temporal behavior of the plasma current induced by the short-pulsed (3 ns FWHM) electron beam in neutral gas was demonstrated on the basis of the experimental results in the previous paper.[1] On the arrival of the electron beam, first the high-energy beam electrons ionize and excite gas atoms. After the space-charge-neutralization time t_{bn}, plasma electrons resulting from the ionization are accelerated

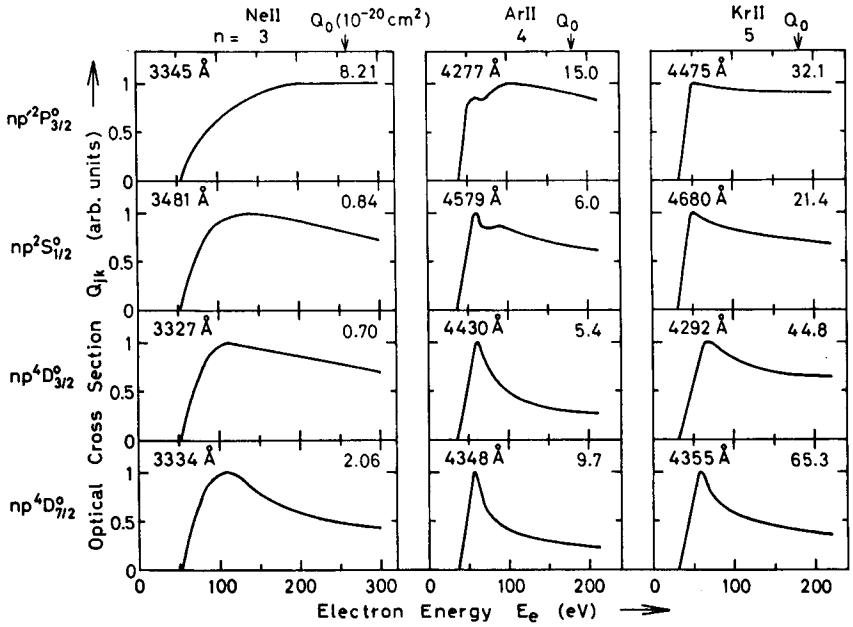

Fig. 9. Optical cross sections $Q_{jk}(E_e)$ of the several NeII, ArII, and KrII lines from np′ and np levels. The values Q_0 are the absolute values at their maxima.

by the axial electric field induced by the large $\partial B_\theta/\partial t$ of the azimuthal magnetic field B_θ of the electron-beam current. Then electron avalanching occurs at t_a (breakdown time), and the axial plasma current grows up so that its growth makes $\partial B_\theta/\partial t$ small. In this period, the induced electric field becomes low, and plasma electrons thermalize themselves under the balance between the energy gain resulting from resistive dissipation of the plasma current and the energy loss due to ionization and excitation of gas atoms. The thermalized plasma lasts for a rather long time after t_{bf} (the beam full width of 6 ns, $t_{bn}<t_a<t_{bf}$). From the above modeling of the plasma-current production, the effective or averaged plasma-electron energy is considered to be high in the period between t_{bn} and t_a, and to be low in the thermalized plasma after t_a.

The quantities $I_{jk}\lambda$ $(=A_{jk}n_jhc)$ are plotted against the Q_{jk} values at $E_e=150$ eV in Figs. 10(a) and (b) for the NeII and ArII lines and for the KrII and XeII lines, respectively, using the I_{jk} values in Table II. The values Q_{jk} of the NeII, ArII, KrII, and XeII lines are given by Walker *et al.*,[48] Feltsan *et al.*,[50] Rostovikova *et al.*,[54] and Rostovikova *et al.*,[55] respectively. Here, it is assumed that the line emissions at their peaks of the initial fast rises are excited between t_{bn} and t_a, and that the effective plasma-electron energy is high enough above the threshold E_{eT} ($E_e=150$ eV) to give rise to the simultaneous ionization and excitation. The relation of eq. (1) holds

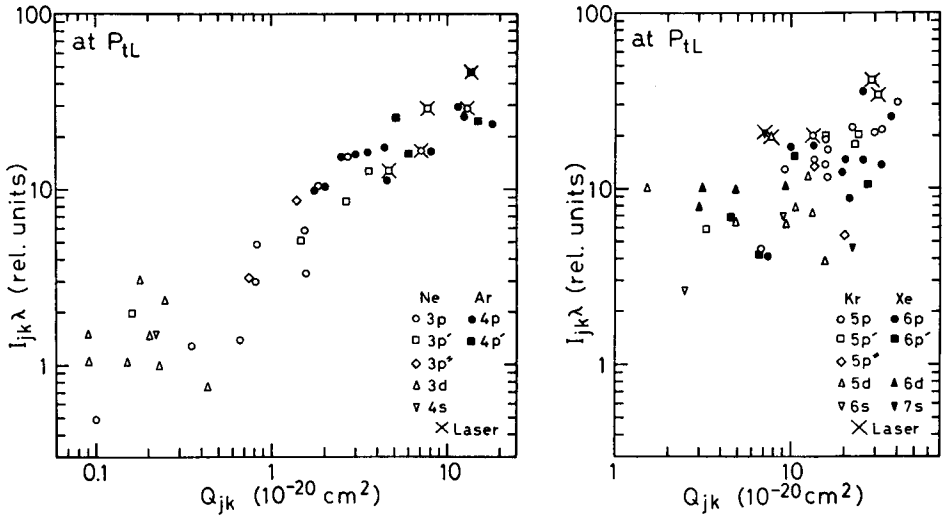

Fig. 10. Quantities $I_{jk}\lambda$ against Q_{jk} values at E_e=150 eV for (a) the NeII and ArII lines and (b) the KrII and XeII lines, using I_{jk} values in Table II.

approximately for the NeII and ArII lines in Fig. 10(a), but this relation is not seen clearly for the KrII and XeII lines in Fig. 10(b). The above results are considered to be affected partly by the time response of about 3 ns of the present measurements, and partly by the uncertainty of Q_{jk} values. Reliable data on $Q_{jk}(E_e)$ are not available, especially for KrII and XeII lines. The laser lines in Table I belong to the group of lines which have large Q_{jk} values for the energetic electrons.

From the above discussions, it is very plausible that the upper levels of the singly-ionized atomic lines are populated by simultaneous ionization and excitation due to energetic plasma-electron impact in the early period between t_{bn} and t_a of the electron-beam pulse. The self-terminating laser emissions have a short pulse of a FWHM of 3 ns or less, and travel along with the electron-beam pulse of about 3 ns FWHM. Accordingly, it is also plausible that the laser emissions are excited in this short time region. For each gas species, the laser emissions show their intensity maxima at the pressure $P_{lM}=(P_{lM})_{end\text{-}on}$ to be different from the pressure $P_{tL}=(P_{lM})_{side\text{-}on}$, at which the intensity maxima appear on the emissions in the direction of side-on view. Further investigations are now in progress to reveal the detailed processes for the laser excitations.

References

1) K. Ono: Jpn. J. Appl. Phys. **18** (1979) 2263.
2) J. E. Rizzo: J. Appl. Phys. **40** (1969) 4883.
3) P. S. P. Wei, J. L. Adamski and J. R. Beymer: J. Appl. Phys. **48** (1977) 568.
4) J. P. VanDevender, J. D. Kilkenny and A. E. Dangor: Phys. Rev. Lett. **33** (1974) 689.

5) J. P. VanDevender, J. D. Kilkenny and A. E. Dangor: J. Appl. Phys. **47** (1976) 1955.
6) J. D. Sethian, D. A. Hammer, K. A. Gerber, D. N. Spector, A. E. Robson and G. C. Goldenbaum: Phys. Fluids **21** (1978) 1227.
7) G. C. Goldenbaum, W. F. Dove, K. A. Gerber and B. G. Logan: Phys. Rev. Lett. **32** (1974) 830.
8) C. A. Kapetanakos, W. M. Black and K. R. Chu: Phys. Rev. Lett. **34** (1975) 1156.
9) C. A. Kapetanakos, W. M. Black and C. D. Striffler: Appl. Phys. Lett. **26** (1975) 368.
10) D. A. Hammer, K. A. Gerber, W. F. Dove, G. C. Goldenbaum, B. G. Logan, K. Papadopoulos and A. W. Ali: Phys. Fluids **21** (1978) 483.
11) C. W. Werner and E. V. George: *Principles of Laser Plasmas*, ed. G. Bekefi (John Wiley & Sons, New York, 1976) Chap. 10, p. 421.
12) *Excimer Lasers*, ed. C. K. Rhodes (Springer-Verlag, Berlin, 1979).
13) R. W. Rreyfus and R. T. Hodgson: J. Vac. Sci. & Technol. **10** (1973) 1033.
14) R. W. Dreyfus and R. T. Hodgson: Phys. Rev. **A9** (1974) 2635.
15) J. J. Kim, G. Baer and R. N. Dexter: Phys. Rev. **A13** (1976) 1115.
16) R. W. Dreyfus: Appl. Phys. Lett. **29** (1976) 348.
17) R. W. Dreyfus and R. T. Hodgson: Appl. Phys. Lett. **20** (1972) 195.
18) E. L. Patterson: J. Appl. Phys. **44** (1973) 3193.
19) A. Luches and M. R. Perrone: J. Appl. Phys. **46** (1975) 4829.
20) K. Ono: Jpn. J. Appl. Phys. **18** (1979) 1013.
21) A. R. Striganov and N. S. Sventitskii: *Tables of Spectral Lines of Neutral and Ionized Atoms* (Plenum Press, New York, 1968).
22) C. S. Willett: *Introduction to Gas Lasers: Population Inversion Mechanisms wish Emphasis on Selective Excitation Processes* (Pergamon Press, Oxford, 1974) p. 405.
23) R. Beck, W. Englisch and K. Gürs: *Tables of Laser Lines in Gases and Vapors* (Springer-Verlag, Berlin, 1976).
24) J. D. Shipman: Appl. Phys. Lett. **10** (1967) 3.
25) D. M. Clunie, R. S. A. Thorn and K. E. Trezise: Phys. Lett. **14** (1965) 28.
26) K. G. Ericsson and L. R. Lidholt: IEEE J. Quantum Electron. **QE-3** (1967) 94.
27) D. A. Leonard: IEEE J. Quantum Electron. **QE-3** (1967) 133.
28) O. Andrade, M. Gallardo and K. Bockasten: Appl. Phys. Lett. **11** (1967) 99.
29) D. A. Leonard and W. R. Zinky: Appl. Phys. Lett. **12** (1968) 113.
30) A. A. Isaev and G. G. Petrash: Sov. Phys. -JETP **29** (1969) 607.
31) F. A. Korolev, G. V. Abrosimov, A. I. Odintsov and V. P. Yakunin: Opt. & Spectrosc. **28** (1970) 290.
32) G. V. Abrosimov: Opt. & Spectrosc. **31** (1971) 54.
33) F. A. Korolev, G. V. Abrosimov and A. I. Odintsov: Opt. & Spectrosc. **33** (1972) 399.
34) G. J. Linford: IEEE J. Quantum Electron. **QE-8** (1972) 477.
35) J. H. Sanders and J. E. Thomson: J. Phys. **B6** (1973) 2177.
36) A. I. Odintsov, N. G. Turkin and V. P. Yakunin: Opt. & Spectrosc. **38** (1975) 244.
37) D. A. Leonard: Appl. Phys. Lett. **7** (1965) 4.
38) T. A. DeTemple, T. K. Plant and P. D. Coleman: Appl. Phys. Lett. **22** (1973) 644.
39) K. G. Whitney and J. Davis: J. Appl. Phys. **46** (1975) 4103.
40) R. I. Rudko and C. L. Tang: J. Appl. Phys. **38** (1967) 4731.
41) W. L. Wiese, M. W. Smith and B. M. Glennon: *Atomic Transition Probabilities* (U. S. Government Printing Office, Washington, D. C., 1966) Vol. 1.
42) A. V. Loginov and P. F. Gruzdev: Opt. & Spectrosc. **44** (1978) 123.
43) W. L. Wiese, M. W. Smith and B. M. Miles: *Atomic Transition Probabilities* (U. S. Government Printing Office, Washington, D. C., 1969) Vol. 2.
44) N. Spector and S. Garpman: J. Opt. Soc. Am. **67** (1977) 155.
45) M. H. Miller, R. A. Roig and R. D. Bengtson: Phys. Rev. **A8** (1973) 480.

46) S. H. Koozekanani: IEEE J. Quantum Electron. **QE-2** (1966) 770.
47) S. H. Koozekanani: IEEE J. Quantum Electron. **QE-4** (1968) 59.
48) K. G. Walker and R. M. St. John: Phys. Rev. **A6** (1972) 240.
49) J. M. Hammer and C. P. Wen: J. Chem. Phys. **46** (1967) 1225.
50) P. V. Feltsan and M. M. Povch: Opt. & Spectrosc. **28** (1970) 119.
51) I. D. Latimer and R. M. St. John: Phys. Rev. **A1** (1970) 1612.
52) P. N. Clout and D. W. O. Heddle: J. Phys. **B4** (1971) 483.
53) K. I. Rozgachev and A. T. Yaroslavtseva: Opt. & Spectrosc. **28** (1970) 578.
54) G. S. Rostovikova, V. P. Samoilov and Yu. M. Smirnov: Opt. & Spectrosc. **35** (1973) 600.
55) G. S. Rostovikova, V. P. Samoilov and Yu. M. Smirnov: Opt. & Spectrosc. **34** (1973) 3.
56) V. P. Samoilov, Yu. M. Smirnov and G. S. Starikova: Opt. & Spectrosc. **38** (1975) 707.